

Chaotic scattering: An invariant fractal tiling of phase space

Ampawan Tiyapan

Department of Physics, West Virginia University, Morgantown, West Virginia 26506

Charles Jaffé

Department of Chemistry, West Virginia University, Morgantown, West Virginia 26506

(Received 25 May 1995; accepted 16 June 1995)

The existence of an invariant fractal tiling of phase space for unbound Hamiltonian systems is demonstrated. The fractal properties of this partitioning of phase space is intimately related to the redistribution of energy among the various modes of the system. The existence of this tiling enables one to express the expectation values of physical observables as infinite sums over all of the tiles. Furthermore, knowledge of the scaling laws associated with the tiling then enables one to evaluate these sums. © 1995 American Institute of Physics.

I. INTRODUCTION

In the development of classical and semiclassical theories of chemical processes a knowledge of the structure of classical phase space is essential. The structure of phase space for bound systems has been the subject of intense study for the last several decades.¹ More recently, attention has focused on the classical dynamics of unbound systems.² These studies range from fairly esoteric proofs based on abstract models to the numerical exploration of semirealistic model systems. The discussion in this paper is an effort to provide a coherent picture of the geometry imposed on phase space by the dynamics of complex formation. While the process of complex formation is of fundamental interest to chemists, similar processes occur in many other fields. Examples include the trapping of electrons in the tail of the magnetosphere,³ encounters of artificial satellites,⁴ and the dynamics of vortices.⁵ The results presented have implications for these and other applications.

The present study was motivated by the results presented by the authors in a recent paper in this journal.⁶ Reported there are the results of a detailed numerical investigation of the fractal structure of the initial angle–final action plots of an inelastic collision of a helium with an iodine molecule. It was demonstrated there that the formation of the HeI₂ van der Waals complex is a direct consequence of the chaotic nature of the dynamics, that the final action is a fractal function of the initial angle, and the task of characterization of the geometrical properties of the fractal was begun. The fractal structure observed in the initial angle–final action plots reflects the fractal geometry imposed on the classical phase space by the dynamics. It is this fractal geometry of phase space that is the subject of the present paper. It will be demonstrated that the homoclinic tangle,⁷ the occurrence of which is responsible for the chaotic nature of the dynamics, partitions the classical phase space into an invariant fractal tiling, that the fractal properties of this partitioning are of fundamental chemical interest, and that dynamical properties can be expressed as a sum over each of the parts of the partitioning.

It has long been recognized that the dynamics of bound systems can be classified as either regular or chaotic.⁸ The dynamics of unbound systems can be classified in the same

manner.⁹ In both bound and unbound systems the chaotic behavior is a consequence of the existence of a homoclinic tangle.⁷ Despite of this common origin, the manifestations of the chaotic behavior are quite different. The differences are clearly seen in systems possessing a small number of degrees of freedom. As an example, compare the scattering dynamics of atom–diatom collision with the bound dynamics of a triatomic molecule (for total angular momentum equal to zero). In both cases the systems possess three degrees of freedom. In the first case the dynamics are integrable both prior to and after the collision. The integrals of the motion can be taken to be the translational energy of the atom with respect to the diatom, and the vibrational action and the angular momentum of the diatom. It is only during the collision that the dynamics are chaotic. Thus the chaotic behavior only occurs for a finite period of time. This is very different from the bound case where the dynamical behavior is chaotic for all time. There are several important and interesting consequences of this difference. The first of these is that numerical methods used to investigate the dynamics must be modified. The Poincaré surface of section (SOS) is a good example. In bound systems the surface of section is constructed with a single trajectory. As the system evolves, each time the trajectory crosses the SOS, the point of intersection is marked. As the dynamics are bound, in the infinite time limit, the trajectory will cross the SOS an infinite number of times. Thus, a single trajectory will provide a significant amount of detailed information concerning the structure of phase space. For unbound systems, a single trajectory will only cross the SOS a finite number of times before it escapes back to infinite. As a consequence, for unbound systems one must use an intelligently chosen ensemble of trajectories in order to construct the SOS. The actual ensemble that is used will vary depending on the question that one is asking. Another important consequence lies in the nature of the dynamically invariant manifolds associated with the regular motion. In bound systems possessing N degrees of freedom and one global constant of the motion, that is, the energy, the regular dynamics are confined to N dimensional invariant tori embedded in the $2N-1$ dimensional energy shell. Here, in the infinite time limit, the dynamics fills the invariant torus, that is, comes arbitrarily close to all points on the torus. In unbound systems, the regular motion is confined to $2N-1$ dimensional

tiles embedded in the $2N-1$ dimensional energy shell. A single trajectory will not fill a tile, rather, the tiles are filled by a family of trajectories that have the same topology, that is, the trajectories can be deformed into each other in a smooth and continuous manner.

Much of the formal theoretical work on unbound dynamical systems has focused on hyperbolic (purely chaotic) systems. To a large extent this is due to the inherent difficulties associated with the coexistence of elliptic (regular) and hyperbolic dynamics. Unfortunately, the majority of systems of interest in chemistry the dynamics are mixed, that is, one observes both regular and chaotic behavior. As a result, many of the theorems are not applicable in a strict sense, however, they do provide guides to expected behavior.

The discussion in this paper focuses on the structure imposed on a given energy shell by the dynamics of a very simple semirealistic model of the formation of a HeI_2 van der Waals complex. It must be recognized that for different energy shells the details of the structure observed will change. It is expected that the qualitative nature of the structure is the same for different energy shells. The changes in the structure of phase space as a function of energy will be discussed in detail in a subsequent publication.¹⁰

The classical dynamics of the model system used in the present study, a helium atom colliding with a iodine molecule, has been investigated previously.^{11,12} The model system is described in detail elsewhere.^{6,13} The model possesses two degrees of freedom, the vibrational mode of the iodine molecule and the scattering coordinate (the distance between the helium and the center of mass of the iodine molecule). The configuration of the system is restricted to a T shape and the potential energy is constructed as a sum of three two-body interactions. These interactions are taken to be Morse oscillators. The results reported here are for a single energy shell. The energy chosen was that of the 20th excited vibrational state of the iodine molecule.

In Sec. II, we begin the discussion of the structure of the classical phase space of the model system in preparation for the presentation in Sec. III of the results of a numerical investigation of this structure. The underlying Cantor set that is responsible for the fractal behavior is discussed in Sec. IV. The implications of the existence of the fractal structure of phase space for the calculation of the physical observables is discussed in Sec. V.

II. THE STRUCTURE OF PHASE SPACE

For the model system considered,⁶ classical phase space is four dimensional. The system possesses one global constant of the motion, the total energy. Therefore the dynamics are confined to a three-dimensional energy shell. The energy shell is unbound, and thus, of infinite volume. The dynamics on the energy shell can be divided into two classes: the bound and unbound motions. The bound motions are characterized by the fact they are confined to a finite region on the energy shell for all times in the past and future. As the system possesses no potential barriers in the exit channel, these motions are confined by the existence of a dynamical barrier. The unbound motions come in from infinite in the past and escape back to infinite in the future. The unbound motion can

be further divided into two subclasses. In the first, the dynamics have sufficient momentum in the correct direction to overcome the dynamical barrier on the way in and then are trapped by the barrier for a finite time. Eventually, the system finds its way back over the barrier and escapes. This is the process of complex formation. In the second subclass of unbound motion, the dynamics are not trapped by the barrier and consequently escape immediately back to infinite. The dynamics belonging to this subclass corresponds to direct collisions.

Both the bound and unbound dynamics fill three-dimensional volumes and cover the energy shell (that is, come arbitrarily close to every point on the energy shell). In addition to these two classes of dynamics, there is a third class. The dynamics belonging to this class fills a volume on the energy shell of dimensionality less than three and is of measure zero. It is this class of dynamics that is responsible for the fractal structure of phase space. This class consists of the unstable periodic orbits and the associated homoclinic and heteroclinic orbits. These homoclinic and heteroclinic orbits are asymptotic, in both the past and future, to the unstable periodic orbits. The homoclinic orbits are asymptotic to the same unstable periodic orbit in both the future and the past, whereas the heteroclinic orbits are asymptotic to different unstable periodic orbits. The importance of these orbits is that the bound and unbound dynamics must interweave themselves around these orbits. This third class of dynamics is the chaotic component. Unfortunately, as the chaotic component is of measure zero, it is very difficult to investigate it directly.

The most important unstable periodic orbit corresponds to the helium sitting at rest at infinite and the iodine molecule vibrating. That is, both the kinetic and potential energy of the helium are zero. The slightest perturbation of this motion results in the helium coming in from infinity, interacting with the iodine molecule and then returning to infinity. This periodic orbit will be called the principle unstable periodic orbit (PUPO), and will be recognized as a periodic orbit dividing surface (PODS).¹⁴ Consider the Poincaré surface of section defined by the PUPO, i.e., $R = \infty$, $P_R \leq 0$, and $H = E$, where R and P_R are the coordinate and conjugate momentum of the helium with respect to the center of mass of the iodine molecule. In this SOS, which is shown in Fig. 1, the PUPO corresponds to the classical boundary (the boundary between the classically allowed and forbidden regions). There is a one-to-one correspondence between the points in this SOS and the incoming scattering trajectories. Thus, the area enclosed by the PUPO is a measure of the number of scattering trajectories and is equal to the classical action of the PUPO. On this SOS the Hamiltonian is separable and can be written as the sum of two parts; the first being the kinetic energy of the helium, and the second being the vibrational Hamiltonian of the iodine molecule. Consequently, the partitioning of the energy between the two degrees of freedom is a local constant of the motion on the SOS. The three dashed curves and the central point in Fig. 1 are locus of points characterized by a particular partitioning of the energy. The central dot corresponds to all of the energy in the translational motion of the helium atom, and the three curves correspond to $\frac{3}{4}$, $\frac{1}{2}$, and $\frac{1}{4}$ of

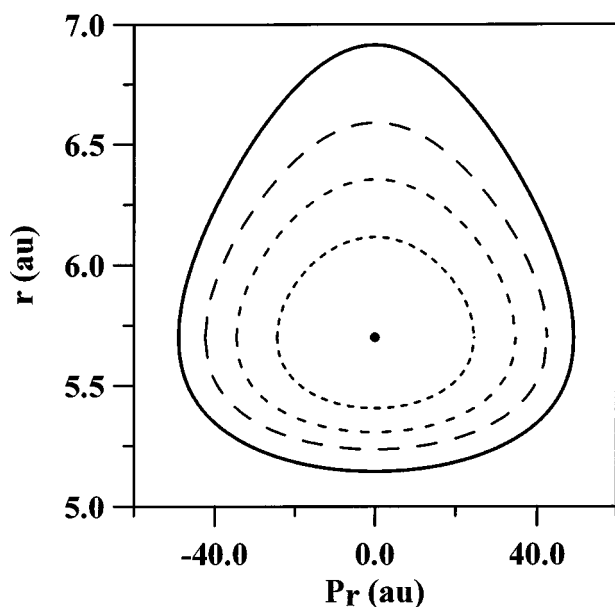


FIG. 1. Shown here is the Poincaré surface of section defined at $R=\infty$, $P_R \leq 0$, $H=E$. The classical boundary is the periodic orbit at $R=\infty$ and all points interior to this orbit correspond to scattering trajectories. In this region of phase space two constants of the motion exists, the total energy and the vibrational action of the oscillator. The dashed curves represent phase space configurations for given values of these two constants of the motion.

the energy in the vibrational mode. This SOS is the space of initial conditions for the scattering trajectories of the system.

Next consider the SOS defined by $R=\infty$, $P_R \geq 0$, and $H=E$. This SOS has the same structure as the SOS just discussed. The PUPO is the boundary of the SOS. The points within the boundary correspond to the outgoing scattering trajectories. It is important to recognize that there is a one-to-one correspondence between the points on these two SOS.

The question of fundamental interest is how the points of the first SOS are mapped into those of the second SOS. To address this question consider the SOS defined by $R=R_0$ and $P_R \leq 0$, where R_0 is finite but sufficiently large that the interaction between the helium and the iodine molecule can be neglected (see Fig. 2). Again, the Hamiltonian can be written as a sum of the two parts; the first being the Hamiltonian of the helium and the second the Hamiltonian of the iodine molecule. The classical boundary of this SOS is found by setting $P_R=0$. The classical boundary of this SOS is not a periodic orbit. The area enclosed within the boundary is larger than that of the SOS defined at $R=\infty$. This is due to the fact that, first, scattering trajectories can cross this surface more than once, and second, bound trajectories can also cross it. Since the SOS is defined in a region of coordinate space where the coupling between the translational motion of helium and the vibrational motion of the iodine molecule can be neglected there will exist an additional local constant of the motion. This local constant of the motion can be taken to be the vibrational energy or, equivalently, the vibrational action of the iodine molecule. Its existence can be used to partition the SOS into two parts. Consider the locus of points defined by the vibrational energy of the iodine molecule being equal to the total energy, or equivalently, the kinetic and potential

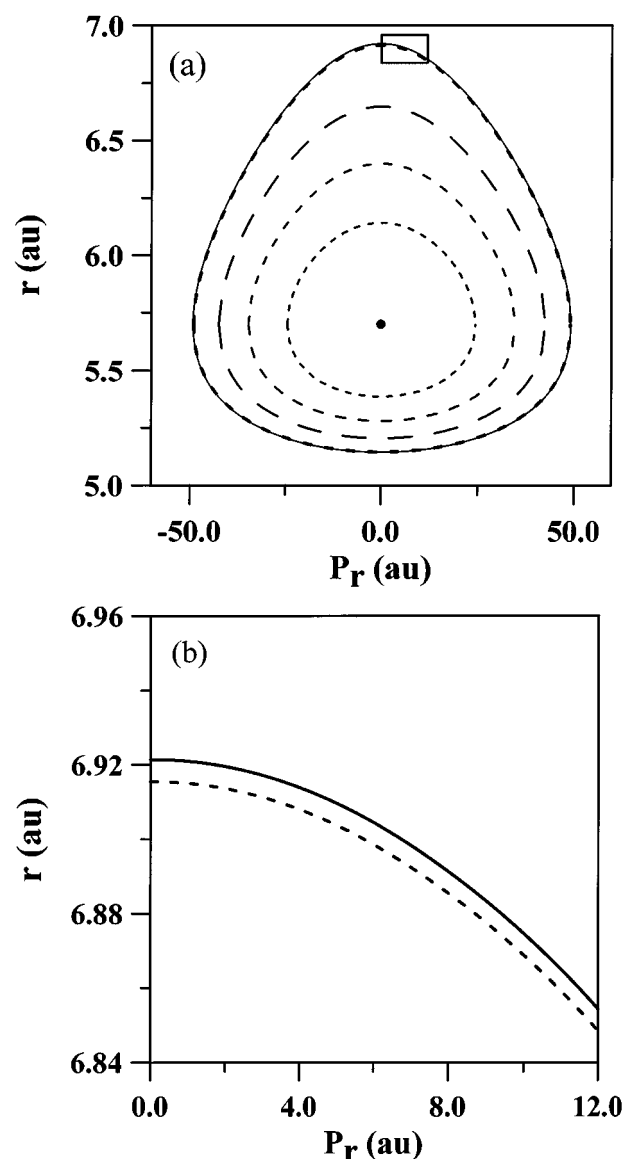


FIG. 2. Shown here is the Poincaré surface of section defined by $R=R_0$, $P_R \leq 0$, $H=E$, where R_0 is sufficiently large that the interaction between the He atom and the iodine molecule can be ignored. In (a) the classical boundary is found by setting $P_R=0$ and the dashed curves correspond to phase space configurations for given values of the two constants of the motion. The dashed curve that appears to be superimposed on the classical boundary is the unstable manifold of the periodic orbit at infinite; it is interior to the boundary. In order to make this clear, the region interior to the rectangle is shown in (b). The first intersection of all scattering trajectories with this surface of section occur interior to the unstable manifold.

energy of the helium being equal in magnitude but opposite in sign. This locus of points is shown in Fig. 2(a) as a dashed line that appears to be superimposed on the classical boundary. An expansion of the small rectangle is shown in Fig. 2(b). Here it is clear that this locus of points are inside the classical boundary. By propagating this locus of points backward in time, it is clear, due to the existence of the additional local constant of the motion, that it is asymptotic in the infinite past to the PUPO. Since classical trajectories cannot intersect in phase space, the points interior to this locus of points correspond to the first intersections of the scattering

trajectories with the SOS. Consequently, the area enclosed by this locus of point must be equal to the area of the SOS at infinity. This is easily verified by comparing the action integral over this locus of points with the action integral over the unstable periodic orbit at infinity. The points exterior to this locus of points correspond to bound trajectories and multiple crossing of the SOS by the scattering trajectories.

Unstable periodic orbits possess stable and unstable manifolds.⁷ The dynamics asymptotic to the unstable periodic orbit in the future are confined to the stable manifold, while the dynamics asymptotic to the unstable periodic orbit in the past are confined to the unstable manifold. The locus of points described above represents the first intersection of the unstable manifold of the PUPO with this SOS. Similar arguments can be made for the structure of the SOS defined by $R=R_0$ and $P_R \geq 0$, with the difference being that now the locus of points represent the last intersection of the stable manifold of the PUPO with the SOS. The two surfaces of section at $R=R_0$ will be called, respectively, the incoming and outgoing surfaces of section. Consider these two loci of points; one representing the unstable manifold and the other the stable manifold. Propagate the unstable manifold on the incoming SOS forward in time and the stable manifold on the outgoing SOS backward in time. The result is two dynamically invariant tubes in the energy shell. These objects are of codimension 1 and partition the energy shell. The points inside these two tubes correspond to scattering trajectories. If these two tubes join smoothly, then the dynamics are regular and the union of the two tubes corresponds to the separatrix that separates the bound from the unbound motion. In such a case no complexes are formed. The generic behavior is that these two tubes do not join smoothly, but rather intersect in a very complicated manner. Each point on the energy shell can be labeled according to whether it is inside (+) or outside (-) the stable and unstable manifolds. There are four possibilities $\{+, +\}$, $\{+, -\}$, $\{-, +\}$, and $\{-, -\}$. The bound trajectories are outside the two manifolds $\{-, -\}$, the scattering trajectories are inside both manifolds $\{+, +\}$. The points on the energy shell that correspond to the remaining two possibilities form a set of measure zero. They correspond to trajectories that are trapped in a finite volume of the energy shell in either the past $\{-, +\}$ or in the future $\{+, -\}$.

The two invariant tubes, which are the stable and unstable manifolds, are two dimension objects embedded in the three dimensional energy shell. The intersections of these two manifolds are a set of one dimensional objects. As the two manifolds are dynamically invariant, the intersections must also be dynamically invariant. These intersections are classical trajectories. Since they are confined to both the stable and unstable manifold, they are homoclinic to the PUPO.

The question of interest now becomes how does the interior of the unstable manifold in the incoming SOS map into the interior of the stable manifold in the outgoing SOS. To answer this question, propagate the unstable manifold forward in time. One observes that the first time that it intersects the outgoing SOS that a single segment of the unstable manifold intersects the region interior to the stable manifold. This is shown schematically in Fig. 3. The closed curve in-

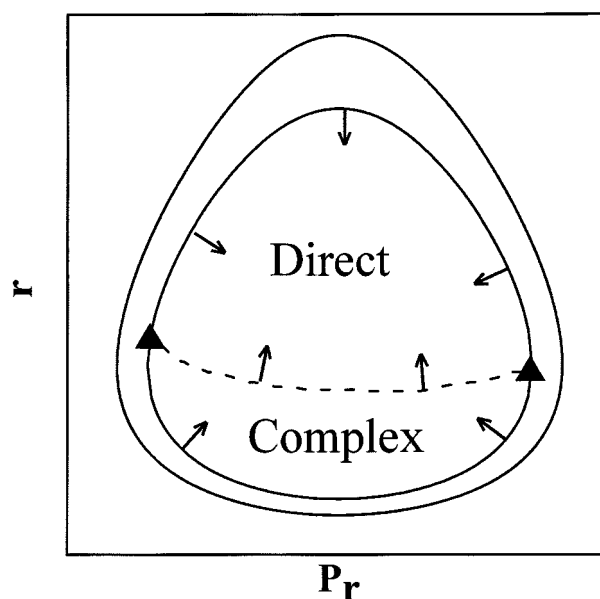


FIG. 3. Shown here is a diagram representing the outgoing surface of section defined by $R=R_0$, $P_R \geq 0$, $H=E$. The closed curve interior to the classical boundary is the last intersection of the stable manifold of the period orbit at infinity. The phase space configurations interior to this curve represent the last intersections of the scattering trajectories with this surface of section. The first intersection of the unstable manifold interior to the stable manifold partitions the scattering trajectories into the direct and complex forming trajectories.

side the classical boundary is the stable manifold, the dashed line partitioning the region interior to the stable manifold is the first intersection of the unstable manifold with the outgoing SOS. The two triangular points are the intersections of the stable and unstable manifolds, and thus, are homoclinic trajectories. These two orbits play a special role in the dynamics and are called the principle intersection points (PIP). The orientations of the unstable and stable manifolds are indicated by the arrows in Fig. 3. The region interior to both the stable and unstable manifold are the direct scattering trajectories. The region interior to the stable manifold and exterior to the unstable manifold are the complex forming trajectories. This region is further partitioned by subsequent intersections of the unstable manifold with the outgoing SOS. On the next intersection another segment of the unstable manifold intersects the interior of the stable manifold. On the third intersection, two additional segments of the unstable manifold intersect the interior of the stable manifold. This process continues *ad infinitum* and the number of segments of the unstable manifold that intersect the interior of the stable manifold increases exponentially. With a few special exceptions, the segments of the unstable manifold that intersect the interior of the stable manifold occurs in pairs. This is shown schematically in Fig. 4. Here it is seen that such a pair further partitions the complex forming region of the outgoing surface of section. The arrows indicate the orientation of the manifolds. The volume interior to this strip is interior to both manifolds and will not be further partitioned. Subsequent intersections will partition the regions exterior to this strip. In the infinite time limit these strips will cover the complex forming region.

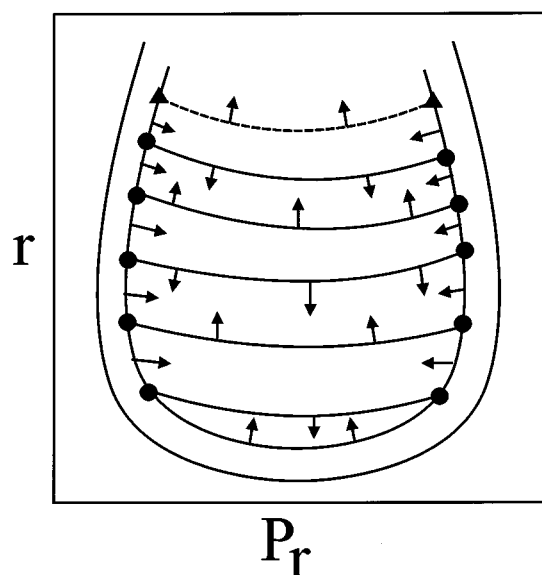


FIG. 4. Shown here is a diagram representing the complex forming region of the outgoing surface of section defined by $R=R_0$, $P_R \geq 0$, $H=E$. The intersections of the unstable manifold of the periodic orbit at infinite partition this region into tiles. Each of these tiles corresponds to complex forming trajectories with different topological behavior.

Consider the boundary of a strip shown in Fig. 4. It is constructed of four segments, two belonging to the stable manifold and the other two to the unstable manifold. The vertices where these segments join are homoclinic orbits. Since the number of strips is exponentially large, the number of homoclinic orbits will also be exponentially large. The area of a strip can be obtained as the action integral over the boundary. As the action integral is invariant with respect to continuous deformations on dynamically invariant surfaces, that is, the stable and unstable manifolds, one can show that this area is also equal to the sums and differences of the action integrals along the homoclinic orbits.¹⁵ The sum of the areas of all the strips is equal to the area interior to the stable manifold. Thus one sees that the last intersection of the unstable manifold with outgoing SOS partitions the region interior to the stable manifold.

Propagating this partitioning of the interior of the stable manifold in the outgoing SOS both forwards and backwards in time enables one to partition the scattering region of the energy shell. This partitioning is an invariant fractal tiling. A tiling is a covering of a space such that the union of all parts, which are called tiles, is the whole space and the intersections of individual tiles are empty. The tiles are obtained by propagating each of the enclosed areas (strips) both forward and backward in time. Clearly, by construction, the tiles are dynamically invariant. That the tiling is a fractal is not yet clear. This is the subject of the remainder of this section.

In order to see that this tiling is a fractal it is necessary to make the connection between the tiling and the initial angle–final action plots. Consider the initial angle–final action plot for the unstable manifold (see Fig. 5). As has been shown in Ref. 6, the final action as a function of the initial angle is a fractal function and its support has fractal dimension δ . This plot is constructed from the same data as used to construct

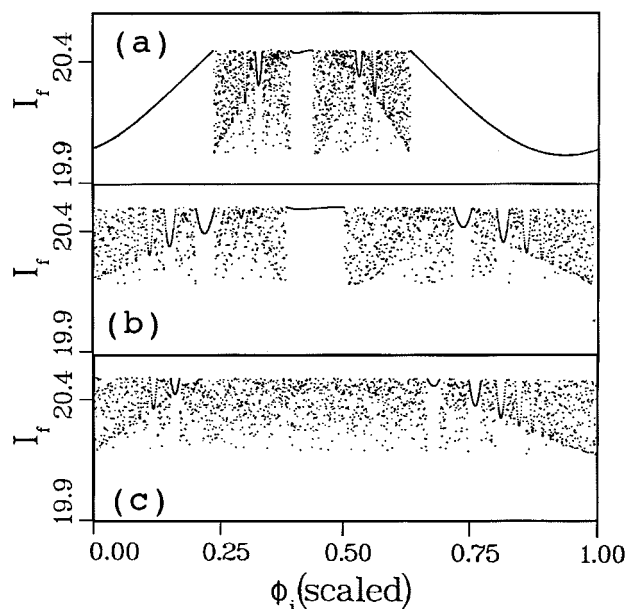


FIG. 5. Shown here is the initial angle–final action plot for the unstable manifold of the periodic orbit at infinity. (a) The full initial angle–final action plot including the direct scattering trajectories. (b) An expansion of the chattering region in (a). (c) Expansion of the gap between the central icicle and the first icicle on the left in (b).

the tiling. Each line segment of the unstable manifold connecting two homoclinic points on the unstable manifold corresponds to an icicle in the initial angle–final action plot. Consequently, the sides of the tile that are constructed from the unstable manifold form a fractal set. Similar arguments are made for the sides of the tiles constructed from the stable manifold. The time-reversal symmetry of the dynamics requires that these two fractal sets be identical. The partitioning constructed in the outgoing SOS is a product of these two fractal sets. Thus it is a fractal and, since dimensions are exponents, has a fractal dimension $\Delta=2\delta$. Propagating this partitioning in time yields the invariant fractal tiling that has a fractal dimension of $\Omega=\Delta+1=2\delta+1$. In Sec. III we present the results of a numerical investigation of the invariant fractal tiling.

We conclude this section observing that the partitioning of the interior of the stable manifold in the outgoing SOS is isomorphic to the invariant fractal tiling of the scattering region of phase space. A quantity of major physical interest is the cross-sectional area of each of the tiles; this area is a measure of the scattering flux that passes through a given tile. A consequence of the fractal properties of the tiling is that these areas and, hence, the flux, obey scaling laws. These scaling laws are obtainable from the fractal properties of the initial angle–final action plots. This is the subject of Sec. III.

III. THE INVARIANT FRACTAL TILING: A NUMERICAL STUDY

In this section the connection between the fractal properties of the initial angle–final action plots and those of the invariant fractal tiling is established. This is accomplished by demonstrating the relationship between the structure of the

initial angle–final action plots and the invariant fractal tiling. The structure of the initial angle–final action plot has been discussed in greater detail in Ref. 6. While this section will start with a brief review of these results, the reader is urged to look there for the full details. It should be noted that the results presented here are constructed from the same data as used in Ref. 6 and thus the numerical results presented here should be considered in conjunction with those reported in Ref. 6.

A. The initial angle–final action plot

The initial angle–final action plot of the unstable manifold is shown in Fig. 5(a). Clearly, the final action is not a well defined, smooth function of the initial angle. The dynamics associated with the smooth portion of this plot correspond to direct collisions; the complex forming collisions are associated with the chattering region. An expansion of the chattering region is shown in Fig. 5(b). The major features seen here are the icicles of the first generation. These icicles correspond to the formation of the (1:*n*) complexes. These complexes survive for a single vibration of the helium, during this period of time the iodine molecule oscillates *n* times. The central icicle corresponds to the formation of a (1:5) complex. The icicles that are on either side of the central icicle correspond to the formation of a (1:6) complex. In general, the *n*th icicle on either side of the central icicle corresponds to the formation of a (1:*n*+5) complex. There exists an infinite number of icicles of the first generation and they accumulate at the edges of the chattering region. Icicles of the second generation are found in the gaps between the icicles of the first generation. An expansion of the first gap to the left of the central feature is shown in Fig. 5(c). The icicles of the second generation correspond to the formation of (2:*n*) complexes. These complexes survive for two oscillations of the helium and *n* oscillations of the iodine molecule. The icicles of the third generation are found in gaps between the icicles of the second generation and correspond to the formation of (3:*n*) complexes. This pattern continues indefinitely. At the *m*th level we find the icicles of the *m*th generation that correspond to the formation of (*m*:*n*) complexes. The icicles are denumerable, that is, they can be labeled in a unique manner. The icicles of the *m*th generation are labeled by *m* signed integers. The first *m*–1 of these identify the family of the *m*th generation to which the icicle belongs, and the last integer identifies the icicle's position within its family. The reader is referred to Ref. 6 for the full details of this labeling system.

The structure of the initial angle–final action plot has been shown to be asymptotically self-similar and its asymptotic fractal properties have been determined.⁶ It possesses two asymptotic scaling laws. The first, called the intragenerational scaling law, describes the scaling of icicles within a given generation; the intragenerational scaling constant was determined as $\alpha=0.9736$. The second, called the intergenerational scaling law, describes the scaling of a family of icicles of one generation into the icicles of the next generation; the intergenerational scaling constant was determined $\beta=0.000\ 164$. With fairly simple algebra, it can be shown

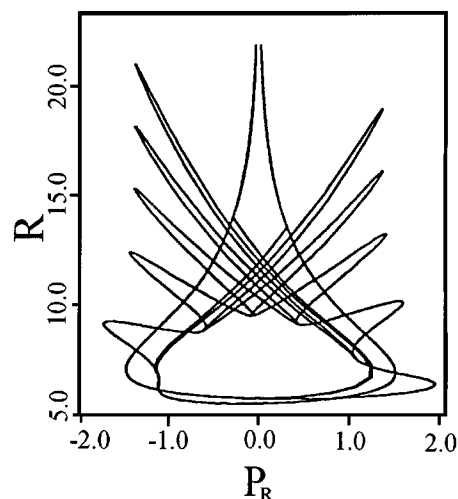


FIG. 6. Shown here is the homoclinic tangle of the stable and unstable manifolds of the PUPO in the surface of section defined by $r=r_e$, $P_r \geq 0$, $H=E$.

that these scaling constants are related to the fractal dimension δ by

$$\alpha^\delta + 2\beta^\delta = 1. \quad (1)$$

Using this relation the fractal dimension was determined, $\delta=0.562$.

B. The homoclinic tangle

The locus of points representing the first intersection of the unstable manifold with the incoming SOS (defined in Sec. II) was used as initial conditions for classical trajectories. These trajectories were followed until they entered the interior of the stable manifold in the outgoing SOS. The SOS defined by $r=r_e$ and $p_r \geq 0$ was constructed. Here, r is the internuclear distance of the iodine molecule and p_r is the conjugate momentum; r_e is the equilibrium distance. This yields a representation of the unstable manifold. The equivalent representation of the stable manifold can also be constructed from this data. First note that the unstable and stable manifolds are time-reversed images of each other. As a consequence, the representation of the stable manifold can be obtained by constructing the SOS defined by $r=r_e$ and $p_r \leq 0$, and then changing the sign of the momentum, $p_r \rightarrow -p_r$. The results of this calculation are shown in Fig. 6. This is the homoclinic tangle of the stable and unstable manifolds of the PUPO. An understanding of this structure is straightforward once the structure of the initial angle–final action plot is understood.

Consider the segment of the unstable manifold that corresponds to direct collisions. This segment is the support of the direct icicle in the initial angle–final action plot of the unstable manifold [see Fig. 5(a)]. The portion of the homoclinic tangle corresponding to this segment is shown in Fig. 7. The area exterior to this closed path corresponds to the direct collisions and is called the direct tile. The area exterior to the direct tile contains the both the bound dynamics and the scattering dynamics characterized by the formation of complexes.

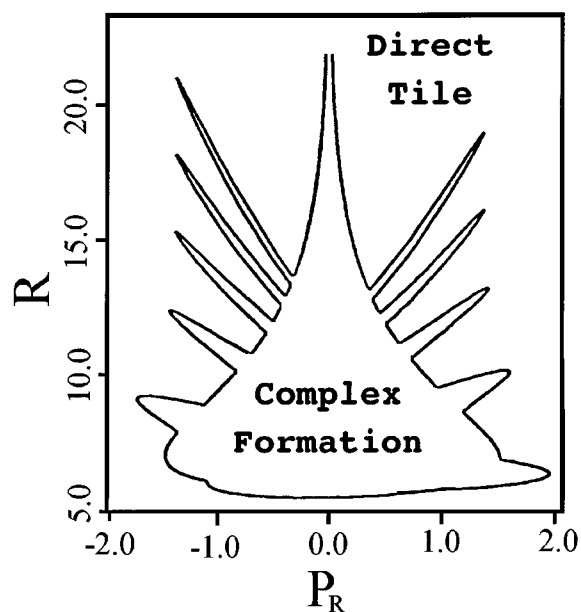


FIG. 7. Shown here is the partitioning of the surface of section defined by $r=r_e$, $P_{ur} \geq 0$, $H=E$ into regions associated with the direct and complex forming trajectories.

Consider the area exterior to the direct tile, that is, the region of complex formation. The large scale structure of this region is shown in Fig. 8. This figure is constructed by plotting the stable and unstable manifolds until they first intersect and then plotting the segments of the manifold corresponding to the direct collisions. The large central region is the interaction region. The configurations within this region correspond to the HeI_2 van der Waals complexes. The lobes attached to the left (right) of the interaction region correspond to the complex forming scattering trajectories prior to (after) the formation (dissociation) of the complex. The lobes on the left (right) are called the reactant (product) lobes. Consider the reactant lobes marked A, B, and C. The dynamics map the points interior to lobe C into lobe B on the next

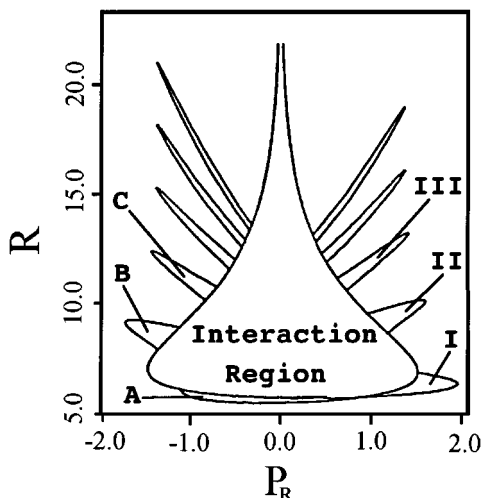


FIG. 8. Shown here is the partitioning of the complex forming region into the interaction region and incoming and outgoing lobes.

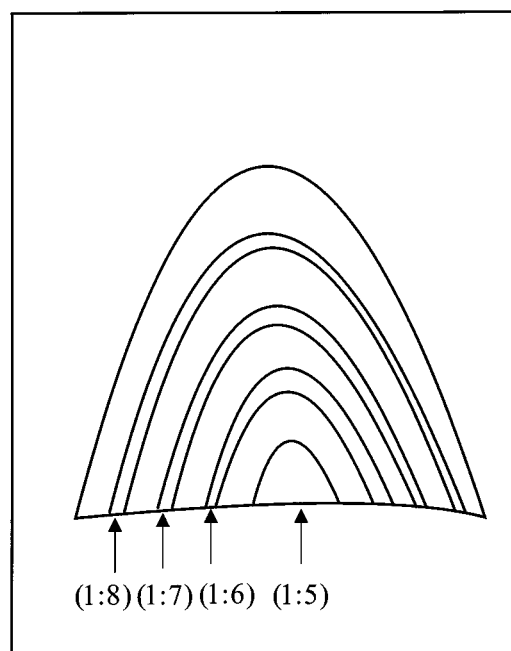


FIG. 9. Shown here is a diagram illustrating the partitioning of an incoming (outgoing) lobe into tiles associated with trajectories characterized by different topological behavior.

intersection with the SOS. Then the points within lobe B are mapped into lobe A. On the third intersection with the SOS, lobe A is mapped into the interior of the interaction region. The dynamics after dissociation of the complex are similar. Consider the product lobes designated by I, II, and III. On dissociation, states interior to the interaction region are mapped into lobe I. On the next intersection lobe I is mapped into lobe II, and then into lobe III. A consequence of these dynamics is that the structure of the interiors of the lobes are isomorphic with each other. It should also be noted that the product and reactant lobes cannot intersect.

Consider lobe I. The base of the lobe is constructed from a segment of the stable manifold that corresponds to the chattering region and the curved part from a segment of the unstable manifold corresponding to the direct icicle. First observe that the dynamics outlined above require that only the unstable manifold intersects this lobe. Furthermore, the only part of the unstable manifold that can intersect with lobe I is the segment corresponding to the chattering region. With this in mind, propagate segments of the unstable manifold corresponding to different icicles until they intersected lobe I. Shown in Fig. 9 is a cartoon to illustrate this result. The segment corresponding to the central icicle forms a little bump in the center of the base of the lobe. The base of this bump is a segment of the stable manifold. Furthermore, it is the segment that corresponds to the formation of the (1:5) complex. All of the configurations interior to this bump correspond to scattering trajectories that result in the formation of the (1:5) complex and is the tile corresponding to the (1:5) dynamics. Next consider the two segments corresponding to the icicles corresponding to the formation of the (1:6) complex. When these segments intersect with lobe I, they form a band over the (1:5) tile. Again, the segments of the stable

manifold forming the base of the band correspond to the formation of a (1:6) complex. The configurations interior to the band correspond to scattering trajectories that result in the formation of the (1:6) complex, and thus this band is the tile associated with the (1:6) dynamics. The other icicles of the first generation continue to follow this pattern, forming a sequence of tiles accumulating at the edge of the lobe.

The icicles of the second generation form a similar pattern. Consider the icicles of the second generation. These icicles form families of tiles in the gaps between the tiles of the first generation. At first sight, one might expect the second generation icicles in the gaps between the (1:5) and the (1:6) icicles to form tiles in the gaps between the (1:5) and (1:6) tiles. However, this is not what occurs; the pattern is more complicated. Consider the (2:11) icicles. There are two of these icicles. They are in the gaps on either side of the central (1:5) icicle. These two icicles form a tile in the gap between the (1:5) and the (1:6) tile. Next consider the (2:12) icicles. There are six of these icicles. The first two are in the gaps between the (2:11) and (1:5) icicles on either side of the (1:5) icicle. These two icicles form a tile in the center of the gap between the (1:6) and (1:7) tiles. The next two (2:12) icicles are in the gaps between the (2:11) and the (1:6) icicles. These two icicles form a tile in the gap between the (1:6) and the (2:11) tiles. The last two (2:12) icicles lie in the gaps between the (1:6) and the (1:7) icicles. These two icicles form a tile in the gap between the (2:11) and the (1:5) tiles. There are ten (2:13) icicles. These icicles form five (2:13) tiles. The first of these is in the gap between the (1:8) and (1:7) tiles. The next two are in the gap between the (1:7) and the (1:6) tiles on either side of the (2:12) tile. The last two are in the gap between the (1:6) and the (1:5) tiles. One of these lies in the gap between the (1:6) and (2:12) tiles and the other in the gap between the (2:12) and the (1:5) tiles. This pattern continues, resulting in a family of (2:n) tiles in each of the gaps between the tiles of the first generation. These second generation tiles accumulate at the edges of each of these gaps. A similar pattern is followed by the icicles of the third and higher generations.

The tiles are denumerable and can be labeled in a manner analogous to the icicles. As we have seen earlier, the boundary of the tiles are constructed from segments of the stable and unstable manifolds that correspond to the icicles in the initial angle–final action plots. Two of these segments form the base of the tile. The icicles corresponding to these segments are labeled by m signed integers. The icicles forming such a pair have the same label with opposite signs. Thus, the first integer in one of the icicles label is positive. This is the label assigned to the tile. Thus, the tiles are labeled by m integers. The last $m-1$ being signed. The tile corresponding to the formation of the (1:5) complex is labeled $[0]$, the next corresponding to the (1:6) complex by $[1]$, etc. For the second generation, the tile labeled $[n_1, 0]$ is the central tile in the gap between the $[n_1]$ and the $[n_1+1]$ tile, and the tile labeled $[n_1, n_2^\pm]$ is the n_2^{th} tile in either the $[n_1]$ side or the $[n_1+1]$ side of the $[n_1, 0]$ tile. In general, the tiles of the m th generation are labeled by m integers $[n_1, n_2^\pm, \dots, n_m^\pm]$. The first $m-1$ integers identify the family, that is, the gap, and the m th integer identifies the position of

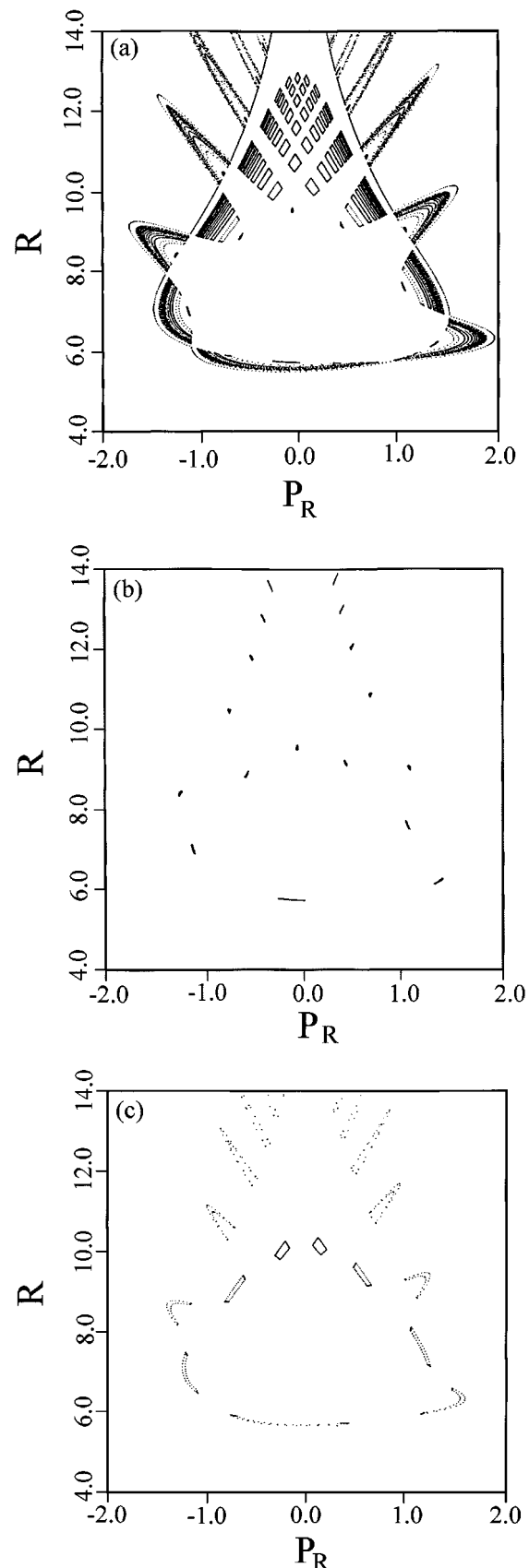


FIG. 10. Shown here is the partitioning of the interaction region by the tiles belonging to the first generation. (a) The first nine tiles of the first generation; (b) the (1:5) tile; (c) the (1:6) tile.

the tile within its family. Using time-reversal symmetry, the same arguments can be applied to the structure of the reactant lobes. Thus, the reactant lobes are also partitioned into an invariant fractal tiling, and the tiles can be labeled in the same manner. However, it must be noted that the resulting labeling system is not the same for the reactant and product lobes. That is, that the dynamics do not map the $[n_1, n_2^\pm, \dots, n_m^\pm]$ tile in the reactant lobes into the $[n_1, n_2^\pm, \dots, n_m^\pm]$ tiles in the product lobes. This is due to the fact that the labeling of the tiles in the product lobes were constructed from the labeling of the icicles on the unstable manifold, while the labeling of the tiles in the reactant lobes is constructed from the labeling of the icicles on the stable manifold. Thus the question of interest becomes which tile in the reactant lobe maps into which tile in the product lobes.

To this point, the discussion has focused on the dynamics exterior to the interaction region. This region is characterized by the fact that none of the trajectories belonging to chaotic component lie within it. The first trajectories encountered belonging to this set are homoclinic orbits of the PUPO and lie on the boundary of the interaction region. As a consequence we consider the interaction region to be the boundary and its interior.

C. The interaction region

The question of interest has now become of how do the tiles in the reactant lobes map into the tiles in the product lobe. The answer to this question lies in the structure of the interaction region. In many respects this is the most important region of phase space. This region of phase space corresponds to the existence of the HeI_2 van der Waal's complex. In principle, a knowledge of the structure of this region of phase space should be sufficient to determine all physical observables of the complex. The dynamics in the interaction region correspond to both complex forming and bound trajectories. The present discussion will focus on the complex forming dynamics. The bound dynamics will be discussed later.

In order to investigate the structure of the interaction region, propagate tiles of the first generation forward to obtain their intersection with the interaction region. This is shown for the first nine tiles in Fig. 10(a). Intersection of individual tiles are shown in Figs. 10(b) and 10(c). In Fig. 10(b) is the [0] or (1:5) tile. This tile intersects the interaction region of the SOS five times, one time for each of the vibrational periods of the iodine molecule during the lifetime of the complex. Shown in Fig. 10(c) are the six intersections of the [1] or (1:6) tile.

Next consider the tiles belonging to the second generation. Illustrated in Fig. 11 are the intersections of the sixteen tiles associated with the formation of the $(2:m)$ complexes for $m=11, 12, 13,$ and 14 . Comparing this figure with Fig. 10(a), one sees that the tile of the second generation lie in the gaps between the tiles of the first generation. Figure 12 shows the (2:11) tile together with the (1:5) and (1:6) tiles. There are three tiles that correspond to the formation of the (2:12) complexes; these are shown in Fig. 13(a). Time-reversal symmetry maps one of these tiles into itself, see Fig. 13(b). The other two (2:12) tiles are mapped into each other

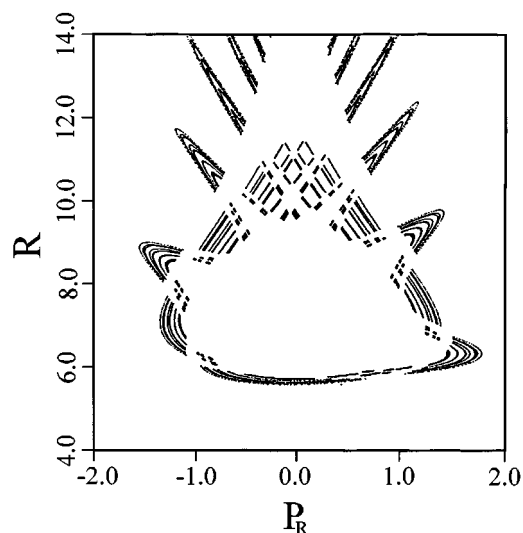


FIG. 11. Shown here are the first sixteen tiles associated with the formation of second generation complexes.

by time-reversal symmetry; these are shown in Figs. 13(c) and 13(d). The mapping of these tiles from the reactant lobe into the product lobe is shown in Fig. 14.

There are five tiles that correspond to the formation of the (2:13) complexes; one symmetric with respect to time-reversal and two time-reversed pairs. This pattern continues indefinitely. In general, there are $2i+1$ tiles corresponding to the formation of a $(2:11+i)$ complex. One symmetric with respect to time-reversal and i time-reversed pairs.

Tiles of the third generation follow a similar pattern. They lie in the gaps parallel to the edges of the tiles of the second generation. This pattern is continued indefinitely, that is, the tiles of the n th generation lie in the gaps between the tiles of the $(n-1)$ th generation. The mapping of the tiles of the third and higher generations from the reactant lobe into the product lobe follow a pattern similar to that of the second generation.

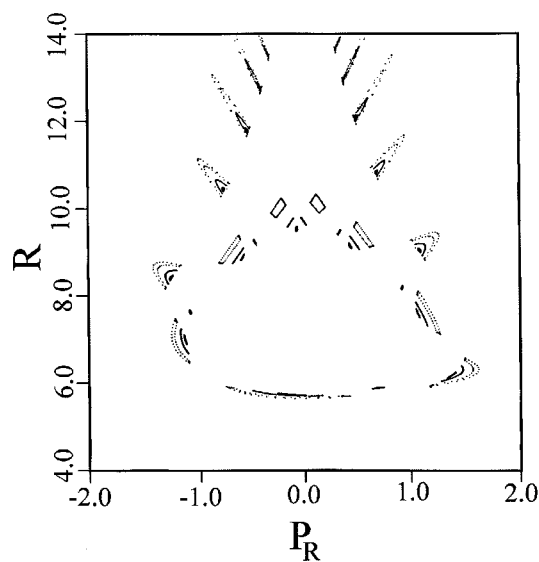


FIG. 12. Shown here is the (2:11) tile together with the (1:5) and (1:6) tiles.

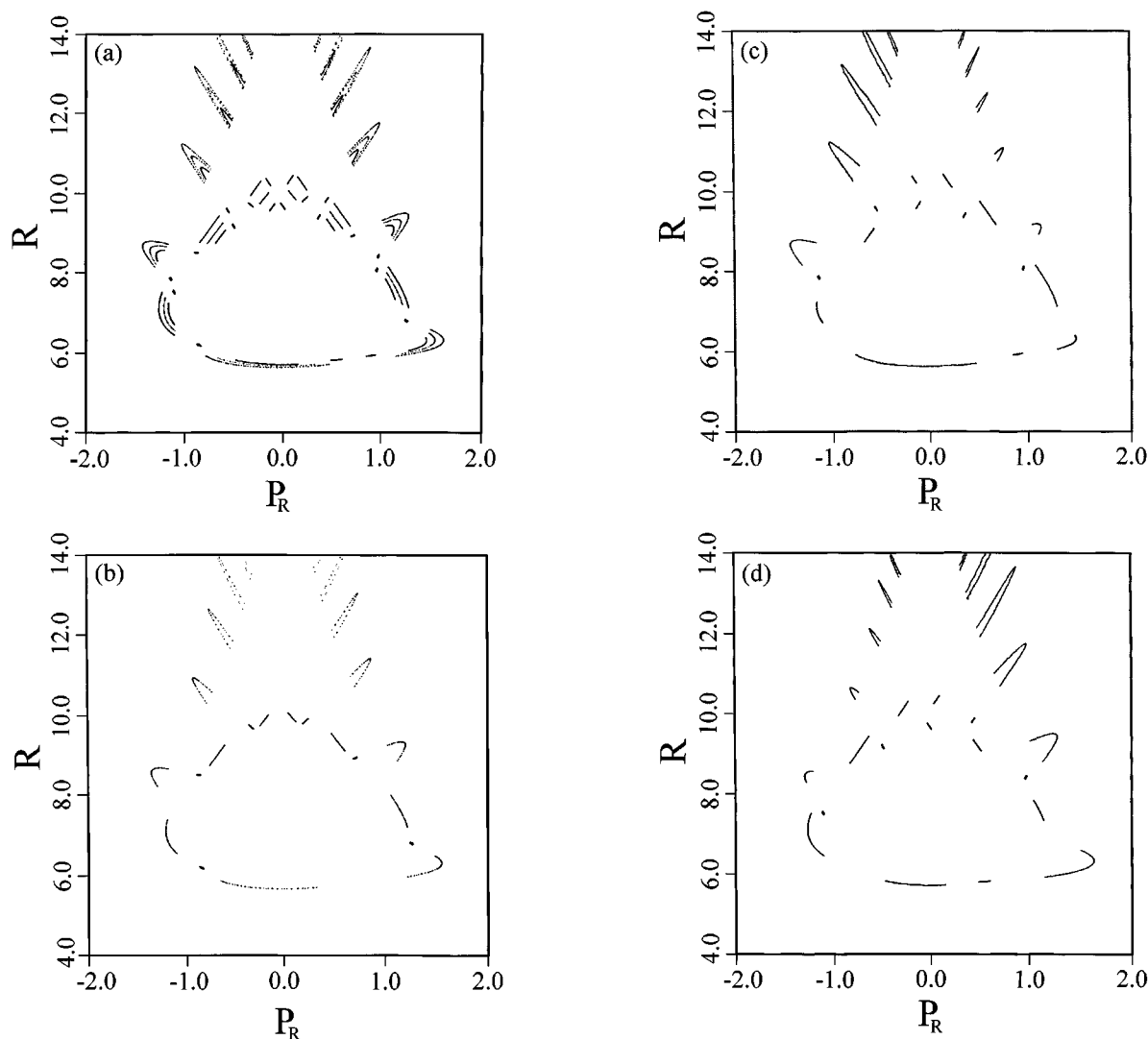


FIG. 13. Shown here are the (2:12) tiles. (a) All three (2:12) tiles. (b) The symmetric (2:12) tile. (c) and (d) The two nonsymmetric (2:12) tiles.

As is discussed at the end of Sec. II, the invariant fractal tiling is a product of two fractal sets, one from the stable manifold and one from the unstable manifold. This is clearly seen in Figs. 10(a) and 11. As a consequence, the scaling of the cross-sectional areas of the tiles can be inferred from the scaling of the icicles observed in the initial angle-final ac-

tion plots. The edges of the tiles are constructed from four segments, two from the unstable manifold and two from the stable manifold. As was seen in Ref. 6, these segments obey to scaling relations, the intragenerational and intergenerational scaling laws. Thus, the areas of the tiles are also expected to obey two scaling laws. The first relates the areas of tiles within a given generation; the intragenerational scaling constant is α . The second relates the areas of one generation with the next generation, the intergenerational scaling constant is β .

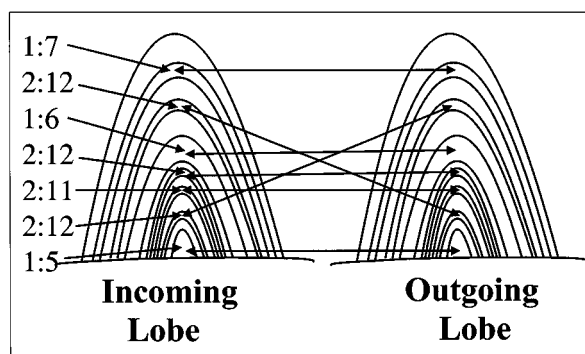


FIG. 14. Shown here is a diagram illustrating the mapping of the tiles from an incoming lobe into an outgoing lobe.

D. The bound dynamics

The first observation concerning the bound dynamics is that while they fill a three-dimensional volume of the energy shell, this volume is not connected. That is, it consists of an infinite number of unconnected pieces. The boundary of each of these pieces is an invariant torus and, thus, each of these pieces has the topology of a solid torus. The bound dynamics within these tori are also extremely complex, that is, chaotic. However, since this complexity is trapped within the bound tori they have no effect on the scattering dynamics and will

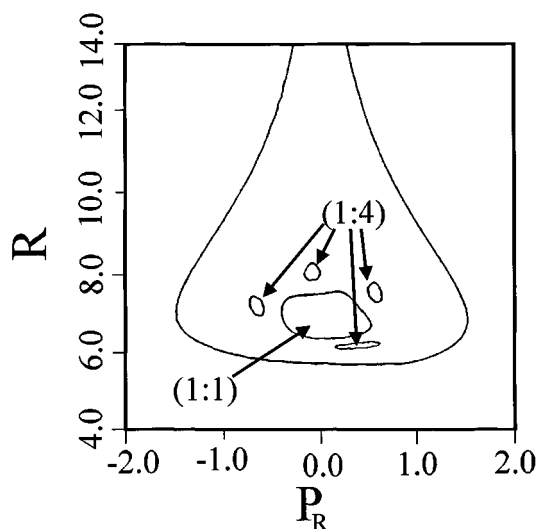


FIG. 15. Shown here are the first two tiles associated with bound motion. The large island is associated with the bound motion surrounding the central periodic orbit and the four island chain is the bound motion associated with the stable (1:4) complex.

not be considered further. The bound tori can be characterized by the periodic orbit that lies at the center of each of the torus. In general, these orbits and the associated bound tori can be labeled by a pair of integers $(k:l)$. Here k is the number of oscillations of the van der Waals' bond, and l is the number of oscillations of the iodine molecule (the ratio k/l is the winding number of the central periodic orbit).

In the present example, the largest bound torus surrounds the (1:1) periodic orbit, see Fig. 15. The configurations within this torus correspond to the existence of a stable van der Waals' complex with two vibrational frequencies that are close equal $\omega_1 \approx \omega_2$. The next largest bound torus surrounds the (1:4) periodic orbit. This torus is wrapped around the (1:1) torus in such a manner that it makes four cycles in one direction while making one in the other direction. The configurations within this torus correspond to the existence of a stable van der Waals' complex with a frequency ratio of ~ 4 . An infinite number of higher order bound tori exist. These tori are wrapped around lower order tori, which in turn are wrapped around even lower order tori. It is this embedding of the bound tori that is responsible for the well known island chain within island chain pattern in the surface of section.

Each of these bound tori is a tile of the invariant fractal tiling of phase space. In general, the $(k:l)$ torus corresponds to the existence of a stable van der Waals' complex with a frequency ratio of k/l . The cross-sectional areas of the bound tiles are expected to obey scaling relationships similar to those observed for scattering dynamics, however, this has not been investigated.

IV. THE CHAOTIC COMPONENT

Associated with the invariant fractal tiling there is an invariant set of measure zero. The elements of this set, which is the chaotic component of the dynamics, are classical trajectories. The importance of this set of orbits is that the in-

variant tiles must interweave themselves around the elements of this set in such a manner as to fill the energy shell; thus, it is responsible for the fractal structure of the tiling. Another important observation is that this set is confined to the interaction region. As a result, the properties of this set are intimately related to the dynamical properties of the van der Waals' complex.

In the language of nonlinear dynamics, the chaotic component is an attractor-repeller. The classical trajectories coming in from infinity are initially attracted to this set of trajectories and then are repelled by it. The actual dynamics with respect to this set are very complicated. This is due to the fact that during the lifetime of the complex a trajectory can be attracted and repelled from many of the elements of the chaotic component. Clearly, the lifetime (and other properties) of the complex will depend on the strength of the attraction/repulsion of the various elements of the chaotic component.

The chaotic component can be constructed in the same manner as the cantor set that underlies the initial angle-final action plots in Ref. 6. Consider the SOS defined by $r=r_e$ and $p_r \geq 0$. First remove the direct scattering tile and the central bound tile. Next remove the tiles of the first generation, then remove the tiles of the second generation. This process is repeated indefinitely. At each successive step remove the tiles of the next generation. In the infinite limit, all of the regular dynamics have been removed and what remains is the chaotic component. The first class of orbits that belong to this set are the unstable periodic orbits. The most important of these is the PUPPO. In addition to this orbit, there exist an infinite number of other unstable periodic orbits. These orbits can be labeled by their winding numbers (n/m) . Here n is the number of oscillations of the van der Waals' bond and m is the number of iodine vibrations. This method of labeling is not unique. There will exist distinct periodic orbits with the same winding number. The unique labeling of the unstable periodic orbits for a mixed system is an unsolved problem.

Another class of orbits belonging to the chaotic component are the homoclinic and heteroclinic orbits. There is an infinite set of homoclinic orbits associated with each of the unstable periodic orbits. These homoclinic orbits are asymptotic in both the past and future to the same unstable periodic orbit. Heteroclinic orbits are asymptotic to different unstable periodic orbits in the future and past.

In addition to the unstable periodic orbits and homoclinic and heteroclinic orbits, a number of other classes of orbits belong to this set. Cantori are an example. These objects, which are the remains of destroyed invariant tori, can be constructed as the limit set of sequences of unstable periodic orbits. One assumes that limits of sequences of homoclinic and heteroclinic orbits associated with the sequences of unstable periodic orbits leading to cantori will yield homoclinic and heteroclinic orbits associated with the cantori. Other strange objects may well exist.

The chaotic component is a very complex collection of some very odd geometrical objects. With the exception of a few very extraordinary cases, very little is understood about the properties of this set. Part of the difficulty in investigat-

ing the structure of this set of orbits is that it is of zero measure, and thus, very difficult to investigate numerically. We have not pursued this problem here, but rather have focused on the consequences of the existence of this set of the regular dynamics.

V. DISCUSSION

The model system considered in this paper was first constructed in an effort to explain the results of a very simple experiment.¹⁶ In the following we consider the results presented here in the light of this experiment. Our goal is not to present a fully developed theory, but rather to illustrate the insight gained from a full understanding of the classical dynamics.

The simple experiment that inspired the model system studied in this paper involved a molecular beam crossed with a laser. The evolution of the system was followed by observing the light that was emitted from the molecular beam. The supersonic molecular beam was formed from helium gas seeded with iodine. In this beam, in addition to the He atoms and the I₂ molecules, there exists a variety of van der Waals' complexes. The most common of these is the species of interest, that is, HeI₂. The frequency of the laser was chosen to excite this complex to a particular vibrational level in the manifold of the first excited electronic state. The states of interest were those with vibrational quanta in the iodine bond. The excited complexes subsequently relaxed back to their ground electronic states. The photons emitted in this process are collected and dispersed. From these observations the disposition of the excess vibrational energy was then determined.

From this experiment it was determined that there is a propensity for a single quantum of vibrational energy to be converted into translational energy. This quantity of energy is sufficient to cause the complex to dissociate into a helium atom and an iodine molecule. An estimate of the lifetime of this process, that is, the redistribution of the energy and the subsequent dissociation, was obtained from the spectral widths of the observed transitions. The experimental results indicate that the redistribution of the energy is not complete nor particularly rapid. That is, this system does not meet the requirements of RRKM theory of unimolecular reactions.

As a consequence of these conclusions, this system has been used extensively to test various non-RRKM unimolecular reaction rate theories. As a result of this interest, a large amount of literature concerning both the classical and the quantum dynamics of this system exists. In the theory of unimolecular reactions it is assumed that the reaction proceeds in two steps. First the molecule is activated and then at some time later it reacts. In the simplest of these theories it is also assumed that rapid and complete redistribution of the vibrational energy occurs in the period of time between the initial activation of the molecule and the reaction. Within this framework it is easy to derive an expression for the microcanonical unimolecular rate constant from purely statistical considerations. The basic idea is to calculate the probability that the energy in the reactive mode exceeds given minimum, E_0 . A triumph of this very simple theory is that it gives the scaling of the rate constant as a function of the total energy,

$$k = c \left(\frac{E - E_0}{E} \right)^s,$$

where the exponent s is the number of vibrational modes, in addition to the reactive mode, of the activated molecule.

In the subsequent development of the theory of unimolecular reactions the requirement that the redistribution is complete is relaxed. In these circumstances, s becomes a parameter to be fitted and is interpreted as the number of degrees of freedom orthogonal to the reactive mode that are involved in the rapid redistribution of the energy. This is very suggestive in the light of the present results. The interaction region in the surface of section shown in Fig. 8 is the phase portrait of the vibrational modes of the activated molecule that are orthogonal to the reactive mode. The redistribution of the energy in these modes occurs due to the existence of the chaotic component of the dynamics. It is tempting to identify the fractal dimension of this component (in this SOS) with the number of orthogonal vibrational modes involved in the redistribution of the energy, that is, $s = \Delta/2 = \delta$. This strongly suggests that scaling behavior of physical observables such as reaction rates are directly connected to the properties of the underlying invariant fractal tiling of phase space. This feature is retained in the further development of unimolecular reaction theory.

Recent developments in the nonlinear dynamics of Hamiltonian systems has spurred the development of non-RRKM theories of unimolecular reactions.^{12,17} The work of Davis *et al.*¹² is characteristic of these developments. They argue that at the lowest level of the theory that the reaction rates can be obtained directly from a knowledge of the partitioning of phase space shown in Fig. 8. At this level of the theory it is assumed that all points in the interaction region have equal probability to react within the next vibrational period. This is in essence the assumption of rapid and complete energy redistribution. This is obviously incorrect if, as in the present case, bound motions exist. However, Davis *et al.* have shown that the difficulties are much more subtle. They have shown that there exist intramolecular bottlenecks that partition the interaction region. These bottlenecks hinder the flow of the energy among the various modes. Davis has developed a statistical theory of unimolecular reaction rates based on this partitioning of phase space.

The intramolecular bottlenecks are the noble cantori, that is, the remains of the most stable invariant tori. These objects are elements of the chaotic component. Their existence implies that the invariant fractal tiling is a multifractal. In other words, that the fractal properties of the tiling will vary depending upon the location in phase space. This is an important point in that it implies that the preparation of the initial state of the activated molecule is critical. The dynamics of different initial states will explore different regions of phase space with different fractal properties. In the present paper we have investigated the asymptotic fractal properties of the tiling. The multifractal properties of the tiling remain to be characterized.

One of the important goals of unimolecular reaction theory is to calculate the unimolecular rate constant, or equivalently, the average lifetime of the activated molecule.

In terms of the invariant fractal tiling, the average lifetime of activated molecule is given by

$$\langle \tau \rangle = \sum_{\text{tiles}} \tau_{\text{tile}} P_{\text{tile}}, \quad (2)$$

where the sum is over all tiles, τ_{tile} is the lifetime associated with a given tile, and P_{tile} is the probability that the system is initial confined to the tile. The sum over all tiles can be written as

$$\sum_{\text{tiles}} = \sum_n \sum_m N_{(n:m)}.$$

The first sum is over the generations and the second is over the families of the tiling and $N_{(n:m)}$ is the number tiles that belong to the m th family of the n th generation. In the present example it is known that the vibrational period of the iodine molecule does not change appreciable during the redistribution of the energy and thus the lifetimes of the tiles are given by

$$\tau_{(n:m)} = m \tau_{I_2},$$

where τ_{I_2} is the period of the iodine vibration. If we assume that all initial states are equally probable, then the probabilities are equal to the cross-section areas of the tiles. The asymptotic scaling laws of these areas are known,

$$P_{(n:m)} = \alpha^{m-5n} \beta^{n-1} P_0.$$

Substituting these results into Eq. (1) yields

$$\langle \tau \rangle = \tau_{I_2} P_0 \sum_n \sum_m N_{(n:m)} m \alpha^{m-5n} \beta^{n-1}. \quad (3)$$

The difficulty in evaluating this sum lies in the numbers $N_{(n:m)}$. For hyperbolic systems an algorithm for these numbers exists, however, such an algorithm is not known for mixed systems. If we assume that in the asymptotic limit they scale as m^{n-1} , then Eq. (2) becomes

$$\langle \tau \rangle = \tau_{I_2} P_0 \beta^{-1} \sum_{n=1}^{\infty} \left(\frac{\beta}{\alpha^5} \right)^n \sum_{m=5}^{\infty} m^n \alpha^m.$$

This sum can be evaluated with a bit of effort.

Our purpose has not been to obtain an expression for the average lifetime but rather to illustrate the role of the fractal partitioning of phase space in determining this quantity. From the aforementioned arguments it is clear that the average lifetime of the complex (and other properties) can be expressed in terms of the fractal properties of the tiling. At the same time it is clear that to do this properly one must understand the multifractal properties of the tiling. We are currently making efforts in this direction.

VI. CONCLUSIONS

It has been demonstrated that the chaotic dynamics in a simple unbound Hamiltonian system can be used to partition the classical phase space. This partitioning is an invariant fractal tiling. A tiling is a covering of a space such that the union of all parts is equal to the full space and that the

intersection of any two parts is empty. The tiling is invariant in the sense that if the system is initially confined to a given tile then it will be confined to this tile for all time. The fractal properties of the tiling are a direct consequence of the existence of the chaotic component of the dynamics.

We have begun the characterization of the fractal properties of this tiling. We have shown that asymptotically this fractal is a two-scale fractal. It is clear that this is a simplification of the true behavior. The fractal is clearly a multifractal. We have also argued that the fractal dimension of this tiling is directly related to the number of degrees of freedom involved in the redistribution of the energy. This is an important result as it will enable one to estimate from theoretical consideration the dimensionality of the manifold of states that are involved in the intramolecular vibrational energy redistribution. We have also shown how the fractal properties of the tiling of phase space can be used to calculate physical observables such as the lifetime of the complex.

ACKNOWLEDGMENTS

This work is supported by the National Science Foundation (Grant No. RII-8922106) and the Pittsburgh Supercomputing Center (Grant No. CHE890031).

- ¹A. J. Lichtenberg and M. A. Lieberman, *Regular and Stochastic Motion* (Springer, New York, 1982).
- ²See articles in *Chaos* **3**(4) (1993).
- ³J. Chen and P. J. Palmadesso, *J. Geophys. Res.* **91**, 1499 (1986); G. R. Burkhart and J. Chen, *ibid.* **96**, 14 033 (1991); **97**, 6479 (1992).
- ⁴J. M. Petit and M. Hénon, *Icarus* **66**, 536 (1986).
- ⁵H. Aref, *Annu. Rev. Fluid Mech.* **15**, 345 (1983); B. Eckhardt and H. Aref, *Philos. Trans. R. Soc. London Ser A* **326**, 655 (1988); B. Eckhardt, *Europhys. Lett.* **105**, 107 (1988).
- ⁶A. Tiyapan and C. Jaffé, *J. Chem. Phys.* **99**, 2765 (1993).
- ⁷S. Wiggins, *Introduction to Applied Nonlinear Dynamical Systems and Chaos* (Springer, New York, 1990).
- ⁸I. C. Percival, *J. Phys. B* **6**, L229 (1973); *J. Phys. A* **7**, 794 (1974); *Adv. Chem. Phys.* **36**, 1 (1977).
- ⁹B. Eckhardt, *Physica D* **33**, 89 (1988), and references cited therein.
- ¹⁰M. Tsuchiya, Ph.D. thesis, West Virginia University, 1995; M. Tsuchiya and C. Jaffé (unpublished).
- ¹¹S. K. Gray, S. A. Rice, and D. W. Noid, *J. Chem. Phys.* **84**, 3745 (1986); D. W. Noid, S. K. Gray, and S. A. Rice, *ibid.* **84**, 2649 (1986); S. K. Gray and S. A. Rice, *Faraday Discuss. Chem. Soc.* **82**, 307 (1986); S. K. Gray, *ibid.* **87**, 2051 (1987); S. B. Woodruff and D. L. Thompson, *J. Chem Phys.* **71**, 376 (1979); G. C. Schatz, V. Buch, M. A. Ratner, and R. B. Gerber, *ibid.* **79**, 1808 (1983); G. Delgado-Barrio, P. Villareal, P. Mareca, and G. Albelda, *ibid.* **78**, 290 (1983).
- ¹²M. J. Davis, *J. Phys. Chem.* **92**, 3124 (1988); S. K. Gray, S. A. Rice, and M. J. Davis, *ibid.* **90**, 3470 (1986); M. J. Davis and S. K. Gray, *J. Chem. Phys.* **84**, 5389 (1986).
- ¹³J. A. Beswick and J. Jortner, *J. Chem. Phys.* **68**, 2277 (1978); *Chem. Phys. Lett.* **49**, 13 (1977).
- ¹⁴E. Pollak, *Theory of Chemical Reaction Dynamics*, edited by M. Baer (CRC Press, Boca Raton, Florida, 1985), Vol. III, p. 123.
- ¹⁵R. S. MacKay, J. D. Meiss, and I. C. Percival, *Physica D.* **13**, 55 (1984); D. Bensimon and L. D. Kadanoff, *ibid.* **13**, 82 (1984); R. S. MacKay, J. D. Meiss, and I. C. Percival, *ibid.* **27**, 1 (1987); I. Dana, N. V. Murray, and I. C. Percival, *Phys. Rev. Lett.* **62**, 233 (1988).
- ¹⁶W. Sharfin, K. E. Johnson, L. Wharton, and D. H. Levy, *J. Chem. Phys.* **71**, 1292 (1973); R. E. Smalley, D. H. Levy, and L. Wharton, *ibid.* **64**, 3266 (1976); M. S. Kim, R. E. Smalley, L. Wharton, and D. H. Levy, *ibid.* **65**, 1216 (1976); K. E. Johnson, L. Wharton, and D. H. Levy, *ibid.* **69**, 2719 (1978).
- ¹⁷M. Zhou and S. A. Rice, *J. Chem. Phys.* **97**, 943 (1992); S. H. Tersigni, P. Gaspard, and S. A. Rice, *ibid.* **92**, 1775 (1990).